THE JOURNAL OF PHYSICAL CHEMISTRY B

Article

pubs.acs.org/JPCB

Asymmetric Profiles and Prewetting Lines in the Filling of Planar Slits with Ne

Salvador A. Sartarelli[†] and Leszek Szybisz*[,‡,§,∥]

[†]Instituto de Desarrollo Humano, Universidad Nacional de General Sarmiento, Gutierrez 1150, RA-1663 San Miguel, Argentina

[‡]Laboratorio TANDAR, Departamento de Física, Comisión Nacional de Energía Atómica, Av. del Libertador 8250, RA-1429 Buenos Aires, Argentina

[§]Departamento de Física, Facultad de Ciencias Exactas y Naturales, Universidad de Buenos Aires, Ciudad Universitaria, RA-1428 Buenos Aires, Argentina

[∥]Consejo Nacional de Investigaciones Científicas y Técnicas, Av. Rivadavia 1917, RA-1033 Buenos Aires, Argentina

ABSTRACT: The filling of slits with identical planar walls is investigated in the frame of the density functional theory. For this kind of slit, the confining potential is symmetric with respect to its central plane. Closed and open systems are studied by applying, respectively, the canonical and grand canonical ensembles (CE and GCE). Results obtained for the confinement of fluid Ne by alkaline surfaces are reported. The behavior of these systems is analyzed by varying the strength of the Ne−substrate attraction, the temperature T, and the coverage Γ_l. It is assumed that the one-body density of the fluid, $\rho(\mathbf{r})$, is uniform along the (x, y) planes parallel to the walls, becoming a function of the coordinate z perpendicular to those planes. Two sorts of solutions are found for the density profile: (i) symmetric ones that follow the left−right symmetry of the potential exerted by the walls and (ii) asymmetric ones that break the symmetry of the slit. The pores are wide enough for determining prewetting (PW) lines and wetting and critical PW temperatures, i.e., T_w and T_{cpw}, from the analysis of symmetric solutions provided by both the CE and GCE schemes. Asymmetric species are examined in detail for $T > T_w$. It is shown that for a given Ne−substrate pair at a fixed T both the CE and GCE frames yield only one asymmetric 2-fold degenerate stable profile (formed by a "thin" wetting film at one wall and a "thick" wetting film at the other) coexisting with two symmetric profiles (formed by "thin" or "thick" wetting films at the two walls), while the remaining asymmetric states are at best metastable. This feature occurs along PW lines and disappears at T_{cpw}.

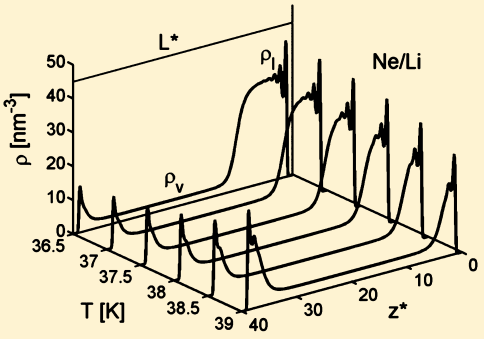

I. INTRODUCTION

The adsorption of fluids on solid walls is connected to physical chemistry (wettability) and to statistical physics (properties of fluids at interfaces, like wetting, spreading, and filling).[1] Theoretical and experimental studies of this subject are of considerable current interest.[2] The behavior of this kind of systems consisting of a liquid phase (l) adsorbed on solid substrates (s) in the presence of a vapor atmosphere (v) depends on the strength of the fluid−fluid (f−f) attraction, ε_{ff}, the well depth of the substrate−fluid (s−f) interaction, $\mathcal{W}_{sf}$, the temperature, T, and the chemical potential, μ. The investigations of this kind of system are not only interesting from the fundamental physics point of view, but they also have numerous technological applications.[3] In the present paper, we shall deal with the formation of films on planar structureless substrates.

A systematic classification of the adsorption on attractive planar surfaces, which exhibit an infinite extent in the x and y directions, was performed by Pandit, Schick, and Wortis.[4] In practice, at a fixed T, the adsorption properties are mainly determined by the relative strength $\varepsilon_r = \mathcal{W}_{sf}/\varepsilon_{ff}$. By varying this parameter, it is possible to sweep a variety of physical phenomena like drying, critical wetting, prewetting, wetting, and layer formation.[4,5]

If a fluid is adsorbed on a single planar wall, the physisorption potential does not exhibit any symmetry along the z axis perpendicular to the (x, y) plane of the substrate. On the other hand, when the confinement is produced by a planar slit with identical walls, the s−f interaction becomes symmetric with respect to the plane located at the slit's center. Under such conditions, it is quite reasonable to expect that $\rho(z)$ would respect the symmetry of the external potential. However, Sikkenk et al.[6,7] have found by carrying out molecular dynamics (MD) calculations that asymmetric density profiles of the fluid may appear in the process of filling a closed planar slit built up of moderately attractive identical walls. This phenomenon was named spontaneous symmetry breaking (SSB). The authors of refs 6 and 7 explained the occurrence of structures with different symmetries in terms of the balance of substrate−liquid γ_{sl}, substrate−vapor γ_{sv}, and liquid−vapor γ_{lv} surface tensions. The SSB has been analyzed over more than two decades.

Received: January 3, 2013
Revised: April 23, 2013
Published: April 25, 2013

   dx.doi.org/10.1021/jp4000895 | J. Phys. Chem. B 2013, 117, 6256−6268

Tang and Harris[8] have also performed MD calculations confirming the finding of Sikkenk et al.[6] Let us remark that both of these MD studies were performed within the frame of the canonical ensemble (CE) statistics, i.e., keeping the number of particles N fixed. Asymmetric solutions have also been found in open systems by Merkel and Löwen.[9] By using both computer simulations and a simple schematic density functional (DF) approach in the frame of the grand canonical ensemble (GCE), these authors demonstrated that under certain conditions a system confined by a symmetric potential can reach a state where the fluid shows a liquid-like density on one side and a vapor-like density on the other side.

More recently, Berim and Ruckenstein[10] have investigated the SSB in symmetric slits by applying a DF formulated for hard spheres (HS) by Tarazona[11] in the smoothed density approximation (SDA). These authors studied in the frame of the CE scheme the confinement of Ar in a slit of solid CO_2 setting the width of the slit, L, at 15 atomic diameters σ_{LJ}. They found asymmetric solutions with lower free energies than that of corresponding symmetric ones in certain ranges of coverage which shrink for increasing temperatures and disappear at a critical temperature T_{ssb}. Subsequent studies of the filling of this kind of slits with classical gases[12−16] confirm that behavior. Furthermore, Berim and Ruckenstein[17] reported asymmetric profiles for quantum ^{4}He confined in closed symmetric planar slits of Cs.

In all the DF−CE calculations mentioned above, the solutions were restricted to films invariant on the (x, y) plane, i.e., assuming $\rho(\mathbf{r}) = \rho(z)$ and excluding drop-like and bridge-like fluid density distributions. Stable drop-like solutions (single pancake) were reported by Mayol et al.[18] for condensation of ^{4}He between parallel Cs plates. These authors fixed the linear density of helium at 70 Å^{-1} and analyzed the behavior as a function of L, finding that for $L \geq 30\sigma_{LJ}$ the most stable phase is the single drop-like configuration that concentrates the whole fluid at one of the walls, while bridge-like structures remain metastable. Furthermore, in the case of inert classical fluids, Berim and Ruckenstein[19] found that for a narrow slit of $L = 10\sigma_{LJ}$ drop-like and bridge-like solutions exhibit lower free energy than the uniform (invariant on the $x-y$ plane) asymmetric profiles for certain ranges of coverage. More evidence for such structures may be found in the works by Rżysko et al.[20] who carried out Monte Carlo simulations ($L = 4\sigma_{LJ}$ and $8\sigma_{LJ}$) and by Edison and Monson[21] who applied a dynamic mean field theory ($L = 6\sigma_{LJ}$). Let us remark that in refs 19, 20, and 21 the width is not sufficiently large to guarantee that the interaction between particles located at different walls be negligible.

Since filling and wetting are related phenomena, our aim is to analyze the connection between the appearance of asymmetric solutions and features of wetting. Therefore, let us now recall some relevant properties of wetting. Given a value of the relative strength ε_r, the results are usually summarized as a phase diagram in the (T, μ) plane; typical examples are depicted in Figure 1 of ref 5. For moderate substrates (i.e., when ε_r is about unity or slightly bigger), there is a first-order wetting transition at the point $[T_w, \mu_w = \mu_0(T_w)]$; here $\mu_0(T)$ is the chemical potential for saturated vapor pressure at temperature T. The wetting temperature T_w lies between the triple point temperature, T_t, and the critical one, T_c, and is characterized by the appearance of coexisting thin and very thick adsorbed fluid films. For $T < T_w$, the coverage of adsorbed films is finite (incomplete wetting), while, for $T \geq T_w$, there is an associated prewetting (PW) line which extends away from the point $[T_w, \mu_0(T_w)]$ into the region of pressures below the corresponding bulk saturation value $P_0(T)$ and terminates at the critical prewetting (CPW) point $[T_{cpw}, \mu_{cpw}]$; see Figure 1b in ref 5. In order to study the PW regime, it is usually assumed that the density profile of the fluid only depends on the coordinate z perpendicular to the substrate, $\rho(\mathbf{r}) = \rho(z)$.[22−26] A PW transition is marked by a jump in the excess surface density (coverage), often expressed in nominal layers l as

$$\Gamma_l = (1/\rho_l^{2/3}) \int_0^\infty dz[\rho(z) - \rho_B] \tag{1.1}$$

where ρ_B is the asymptotic bulk vapor density and ρ_l the liquid density at saturation for a given temperature. The jump occurs between coverages of the thin and thick coexisting wetting films. This discontinuity defined as $\Delta\Gamma_l = \Gamma_l(\text{thick}) - \Gamma_l(\text{thin})$ shrinks for increasing T and eventually vanishes at T_{cpw}, where the coexisting thin and thick wetting films become identical. For more attractive substrates (larger ε_r), the phase diagram presents several convergent PW lines like in the scheme shown in Figure 1d of ref 5 or in the case of the Xe/Li system depicted in Figure 3d of ref 27. For very strong substrates, the coverage increases from zero, either in monolayer steps or continuously.

In simultaneous studies of wetting and filling in the DF−CE scheme, we found some evidence for a correspondence between T_{cpw} of PW lines and T_{ssb} determined for the disappearance of SSB in slits.[14,16] Moreover, Rżysko et al.[20] have also suggested that the SSB is a result of the first-order nature of the transition. If the transition were of the second order, SSB would not occur. A DF with HS described by the fundamental measure theory (FMT) of Rosenfeld−Kierlik−Rosinberg[28,29] has been very recently used in the frame of the GCE for studying confinement of Xe in open symmetrical slits of alkali metals.[27] These DF−GCE calculations provide, in the convex domain of the Helmholtz free energy, asymmetric solutions which are mainly metastable. These results encouraged the present more extended and detailed investigation.

In the present work, we report a systematic search for establishing to what extent PW and SSB are related in the case of the adsorption of Ne on alkali-metal surfaces. The behavior is examined as a function of ε_r and T. The calculations were performed for wetting regimes of adsorption on a single wall. Coincidences and differences between results obtained with the CE and GCE schemes are discussed. It is confirmed that whenever a given adsorbate−substrate pair exhibits a first-order wetting transition then asymmetric profiles appear in the filling of the slit and, in addition, both these phenomena, PW and SSB, terminate at the same temperatures. Moreover, it is shown that, as far as the stable structures are concerned, for both statistics the SSB is reduced to an asymmetric profile coexisting with symmetric wetting films.

The theoretical background together with utilized algorithms is outlined in section II. Section III is devoted to report and analyze the results of our calculations performed in the frames of both the CE and GCE statistics; in addition, it also provides an interpretation of the SSB phenomenon. A review of the findings is given in section IV.

II. THEORETICAL FRAME

The present calculations have been carried out in the frame of the DF theory recently applied for studying physical adsorption

dx.doi.org/10.1021/jp4000895 | J. Phys. Chem. B 2013, 117, 6256−6268

of Ne and Ar.[14−16,30,31] This theory is based on the existence of a grand canonical functional $\Omega(T, \mu, [\rho(\mathbf{r})])$ of the one-particle density $\rho(\mathbf{r})$,[32] which depends parametrically on the two thermodynamic variables T and μ

$$\Omega(T, \mu, [\rho(\mathbf{r})]) = F_{DF}(T, [\rho(\mathbf{r})]) - \mu N \tag{2.1}$$

where F_{DF} is the DF for the Helmholtz free energy and N the number of adatoms

$$N = \int \rho(\mathbf{r})\, d\mathbf{r} \tag{2.2}$$

The equilibrium density profile $\rho_{eq}(\mathbf{r})$ of the adsorbed fluid is obtained by solving the Euler−Lagrange (E−L) equation derived by minimizing (at fixed T and μ) the grand thermodynamic potential

$$\left.\frac{\delta\Omega(T, \mu, [\rho])}{\delta\rho(\mathbf{r})}\right|_{\rho=\rho_{eq}(\mathbf{r})} = 0 \tag{2.3}$$

The value of the functional at equilibrium, $\Omega(T, \mu, [\rho = \rho_{eq}])$, is the real equilibrium grand canonical free energy Ω_{eq}.

II.1. Density Functional. In the DF theory, there is no recipe for an exact expression of the intrinsic free energy F_{DF} corresponding to a fluid immersed in an external potential $U_{sf}(\mathbf{r})$.[33] We adopted the form utilized by Ancilotto and collaborators (see eq 4 in ref 23)

$$\begin{aligned} F_{DF}(T, [\rho(\mathbf{r})]) = {} & \nu_{id} k_B T \int d\mathbf{r}\rho(\mathbf{r})\{\ln[\Lambda^3\rho(\mathbf{r})] - 1\} \\ & + \int d\mathbf{r}\rho(\mathbf{r})\Delta f_{HS}[\overline{\rho}(\mathbf{r}); d_{HS}] \\ & + \frac{1}{2}\iint d\mathbf{r}d\mathbf{r}'\rho(\mathbf{r})\rho(\mathbf{r}')\Phi_{attr}(|\mathbf{r} - \mathbf{r}'|) \\ & + \int d\mathbf{r}\rho(\mathbf{r})U_{sf}(\mathbf{r}) \end{aligned} \tag{2.4}$$

with only one change concerning the effective attractive pair f−f interaction described below. The first term is the ideal gas free energy, where k_B is the Boltzmann constant and Λ is the de Broglie thermal wavelength. Factor ν_{id} was introduced in ref 23 (in the standard theory, it is equal to unity). The second term is the repulsive f−f interaction approximated by a hard-sphere (HS) fundamental measure theory (FMT) functional taken from Kierlik and Rosinberg (KR),[29] which has proven to be very successful even in highly inhomogeneous situations. Here d_{HS} is the HS diameter. The KR version is completely equivalent to the original FMT formulated by Rosenfeld.[28] Notice that in the literature there are more recent versions of the FMT like, for instance, the White Bear proposal[34] where the Mansoori−Carnahan−Starling−Leland[35] bulk equation of state was included. This fact makes the White Bear version more adequate for studying binary mixtures, but in the case of one-component HS fluid, the difference with the original Rosenfeld functional is negligible, as depicted in Figure 3 of ref 34. The third term is the attractive f−f interaction treated in a mean-field approximation (MFA), which is written in terms of a recently proposed version[30] of the separation of the spherically symmetric Lennard-Jones (LJ) 12-6 potential originally introduced by Weeks, Chandler, and Andersen (WCA)[36]

$$\Phi_{attr}^{WCA}(r) = \begin{cases} -\tilde{\varepsilon}_{ff} & r \le r_m \\ 4\tilde{\varepsilon}_{ff}\left[\left(\frac{\tilde{\sigma}_{ff}}{r}\right)^{12} - \left(\frac{\tilde{\sigma}_{ff}}{r}\right)^{6}\right] & r > r_m \end{cases} \tag{2.5}$$

where $r = |\mathbf{r} - \mathbf{r}'|$ and $r_m = 2^{1/6}\tilde{\sigma}_{ff}$ is the position of the LJ minimum. We set $d_{HS} = \tilde{\sigma}_{ff}$. Let us note that Ancilotto et al.[23] adopted for $\Phi_{attr}(r)$ another expression; the advantage of the present one is explained in ref 30. The last contribution to eq 2.4 is due to the adsorbate−substrate interaction.

The well depth $\tilde{\varepsilon}_{ff}$ and the interaction size $\tilde{\sigma}_{ff}$ are considered as free parameters because the use of its standard bare values[22] $\varepsilon_{NeNe}/k_B = 33.9$ K and $\sigma_{NeNe} = 0.278$ nm in the present WCA frame overestimates the experimental result $T_c = 44.49$ K (see Figure 1 in ref 15). The three adjustable parameters (namely, ν_{id}, $\tilde{\varepsilon}_{ff}$, and $\tilde{\sigma}_{ff}$) were simultaneously determined by imposing that on the l−v coexistence curve of Ne at fixed T the data of $\rho_l(T)$, $\rho_v(T)$, and $P_0(T) = P(\rho_l) = P(\rho_v)$ taken from ref 37 be reproduced. In addition, since two bulk phases can coexist at a given T if and only if their chemical potentials are equal at P_0, i.e.,

$$\mu_l(T, P_0) = \mu_v(T, P_0) = \mu_0(T) \tag{2.6}$$

this condition was also imposed. In previous works, we fitted values from Table 3 of ref 38; however, in the present work, we used the output of the NIST Webbook[37] because the latter survey allows one to get data corresponding to non-integer values of T. For determining the optimal $\tilde{\sigma}_{ff}$, all the contributions to the Helmholtz free energy containing this parameter, i.e., all the corresponding terms in both the $\Delta f_{HS}[\overline{\rho}(\mathbf{r}); d_{HS} = \tilde{\sigma}_{ff}]$ and $\Phi_{attr}^{WCA}(r; \tilde{\varepsilon}_{ff}, \tilde{\sigma}_{ff})$ energies, were considered. It is worth noticing that the sets of parameters (ν_{id}, $\tilde{\varepsilon}_{ff}$, and $\tilde{\sigma}_{ff}$) obtained by fitting data of refs 37 and 38 are consistent. The obtained parameter ν_{id} is essentially unity near T_t and decreases to about 0.9 in the regime close to T_c (see Table 1 in ref 15), where there is a well-known departure from the ideal gas behavior.[39] Thus, one can guess that changes in ν_{id} indicate in some way effects of thermal fluctuations which are important mainly close to T_c. On the other hand, since ν_{id} is not strictly unity the Henry's law for adsorption at very low densities[40] is slightly violated in the present formulation. All in all, the present DF version should be considered as a relatively easy phenomenological approach with parameters introduced to account for experimental bulk data.

II.2. Euler−Lagrange Equations. The equilibrium density profile $\rho(\mathbf{r})$ of the fluid is determined from the variational eq 2.3 written as

$$\frac{\delta}{\delta\rho(\mathbf{r})}[F_{DF}[\rho(\mathbf{r}')] - \mu\int d\mathbf{r}'\rho(\mathbf{r}')] = 0 \tag{2.7}$$

This functional minimization leads to

$$\frac{\delta[F_{DF}(T, [\rho(\mathbf{r}')])]}{\delta\rho(\mathbf{r})} = \mu \tag{2.8}$$

This variational condition yields the following E−L equation for a planar geometry

$$\nu_{id} k_B T \ln[\Lambda^3\rho(z)] + Q(z) = \mu \tag{2.9}$$

with

$$Q(z) = \Delta f_{HS}[\bar{\rho}(z);\, d_{HS}] + \int_0^L dz'\rho(z')\frac{\delta\Delta f_{HS}[\bar{\rho}(z');\, d_{HS}]}{\delta\bar{\rho}(z')}\frac{\delta\bar{\rho}(z')}{\delta\rho(z)} + \int_0^L dz'\rho(z')\bar{\Phi}_{attr}(|z - z'|) + U_{sf}(z) \quad (2.10)$$

Here L is the size of the box adopted for solving the E−L equation. In addition, the number of particles by wall area A becomes

$$n = N/A = \int_0^L \rho(z)\, dz \quad (2.11)$$

II.2.1. Grand Canonical Ensemble. In an experimental setup devised to investigate adsorption, the fluid is usually exposed to a reservoir at fixed T_{bath} and P_{bath} (i.e., μ_{bath}), allowing an unrestricted particle exchange with the environment. Under such conditions, the system at thermodynamic equilibrium exhibits fixed V, $T = T_{bath}$, and $\mu = \mu_{bath}$; hence, the adequate procedure for studying such a phenomenon is to apply the GCE statistics. In such a scheme, the E−L equation should be solved by fixing μ and searching for the optimal solutions for $\rho(z)$ and n.

Given a value of the independent variable μ, the density profile may be evaluated by inverting eq 2.9

$$\rho(z) = \frac{1}{\Lambda^3}\exp\left(\frac{\mu - Q(z)}{\nu_{id}k_BT}\right) \quad (2.12)$$

and the self-consistent solution is obtained iterating this relation up to convergence. The number of particles per unit area is calculated with the expression

$$n = \frac{1}{\Lambda^3}\exp\left(\frac{\mu}{\nu_{id}k_BT}\right)\int_0^L dz\, \exp\left(-\frac{Q(z)}{\nu_{id}k_BT}\right) \quad (2.13)$$

II.2.2. Canonical Ensemble. However, in practice, it is usual[10,13,22] to solve the adsorption problem by fixing n together with V and T, that is, by applying the CE scheme, which is much easier to manage numerically than the GCE one. Notice that μ and n are conjugate Legendre variables. In the CE statistics (strictly valid for closed systems), μ is treated as a Lagrange multiplier μ_{ce} to be determined from the solutions together with $\rho(z)$. Thus, in this case, one should solve

$$\frac{\delta[F_{DF}(T, [\rho(z')])]}{\delta\rho(z)} = \mu_{ce} \quad (2.14)$$

which leads to the E−L equation

$$\nu_{id}k_BT\ln[\Lambda^3\rho(z)] + Q(z) = \mu_{ce} \quad (2.15)$$

Then, the density profile $\rho(z)$ can be written as

$$\rho(z) = \rho_0\exp\left(-\frac{Q(z)}{\nu_{id}k_BT}\right) \quad (2.16)$$

with

$$\rho_0 = \frac{1}{\Lambda^3}\exp\left(\frac{\mu_{ce}}{\nu_{id}k_BT}\right) \quad (2.17)$$

Since in the CE scheme the calculations are performed at fixed n, while μ_{ce} is an unknown quantity, then eq 2.17 is used to evaluate μ_{ce} and ρ_0 is obtained from the integrated density profile

$$n = \rho_0\int_0^L dz\, \exp\left(-\frac{Q(z)}{\nu_{id}k_BT}\right) \quad (2.18)$$

which leads to

$$\rho_0 = \frac{n}{\int_0^L dz\, \exp\left(-\frac{Q(z)}{\nu_{id}k_BT}\right)} \quad (2.19)$$

Equating expressions 2.16, 2.17, and 2.19, one gets

$$\rho(z) = \frac{n}{\int_0^L dz\, \exp\left(-\frac{Q(z)}{\nu_{id}k_BT}\right)}\exp\left(-\frac{Q(z)}{\nu_{id}k_BT}\right) \quad (2.20)$$

for the density profile and

$$\mu_{ce} = -\nu_{id}k_BT\ln\left[\frac{1}{n\Lambda^3}\int_0^L dz\, \exp\left(-\frac{Q(z)}{\nu_{id}k_BT}\right)\right] \quad (2.21)$$

for the chemical potential. In this scheme, $\rho(z)$ is determined by iterating eq 2.20 until the required convergence is achieved, and then, μ_{ce} is calculated with eq 2.21.

III. ANALYSIS OF FILLING

Before entering into the analysis of physisorption, we validated the obtained parameters by evaluating the surface tension of the free liquid−vapor interface, γ_{lv}. For such a purpose, we set $U_{sf}(z) = 0$ and followed the procedure outlined in previous works. Along the calculations, dimensionless variables and $z^* = z/\tilde{\sigma}_{ff}$ and $L^* = L/\tilde{\sigma}_{ff}$ for distances, $n^* = N\tilde{\sigma}_{ff}^2/A$ for areal density, and $\rho^* = \rho\tilde{\sigma}_{ff}^3$ for volume density are used.[30,31] Present results for γ_{lv} agree well with experimental data[23,37,41] over the entire temperature range T_t (=24.56 K) $\leq T \leq T_c$ similarly to that displayed in Figure 2 of ref 30.

For the analysis of physisorption, we utilized the *ab initio* potential of Chismeshya, Cole, and Zaremba (CCZ), i.e., $U_{sf}(z) = U_{CCZ}(z)$, given by eq 3 in ref 42 with the potential parameters listed in Table 1 therein. We report here results obtained when slits of Rb, Na, and Li are filled with Ne. This set of substrates exhibits an increasing relative strength, being $\varepsilon_r = \mathcal{W}_{sNe}/\varepsilon_{NeNe} = 0.71$, 1.10, and 1.49, respectively.[30] Let us mention that Sinanoğlu and Pitzer[43] suggested that the strength of the pair f−f potential is modified by interactions with solid substrates. This effect is discussed in detail in ref 44. In the present paper, we neglect the adsorption-induced interactions and, along with other earlier authors,[10,22−26] adopt for studying physisorption the pair f−f potential of eq 2.5 with the empirical parameters $\tilde{\varepsilon}_{NeNe}$ and $\tilde{\sigma}_{NeNe}$ determined in the previous section.

A study of adsorption of Ne on single walls has already been reported in ref 30. In that paper, PW lines and T_w temperatures were determined. Hence, in this work, we shall apply the outlined CE an GCE procedures to examine filling of symmetric pore slits only. In this geometry, Ne atoms are confined by two identical solid walls separated by a distance L. Hence, the s−f interaction becomes $U_{sf}(z) = U_{CCZ}(z) + U_{CCZ}(L - z)$ and repulsion at the walls leads to $\rho(z = 0) = \rho(z = L) = 0$. The reported solutions of the E−L equations were calculated for slits with $L^* = 40$ in the cases of Li and Na and $L^* = 60$ for Rb. These widths are wider than $L^* = 29.1$ adopted for the pioneering molecular dynamics calculations[6] guarantee-

dx.doi.org/10.1021/jp4000895 | J. Phys. Chem. B 2013, 117, 6256−6268

ing that the direct pair interaction between two atoms located close to opposite walls be negligible.

Adsorption isotherms at fixed temperatures, i.e., the reduced chemical potential $\Delta\mu(T) = \mu(T) - \mu_0(T)$ and Γ_l, were calculated using both the GCE and CE schemes. We adopted a step $\Delta T = 0.5$ K for slits of Li and Na and $\Delta T = 0.25$ K for slits of Rb. After describing the method of analysis, we shall first deal with symmetric solutions in order to determine PW lines and wetting temperatures T_w which will be compared with that obtained in the previous study of adsorption on planar surfaces.[30] Next, all symmetric and asymmetric solutions for $T > T_w$ will be examined.

III.1. Method of Analysis. Let us now outline the method of analysis of the adsorption isotherms by describing the treatment of the results obtained when a slit of Li is filled with Ne at a fixed T. For this illustration, we selected $T = 38.5$ K which is the highest temperature exhibiting a van der Waals loop. Data corresponding to symmetric solutions are displayed in Figure 1. In this drawing, the solid lines stand for results

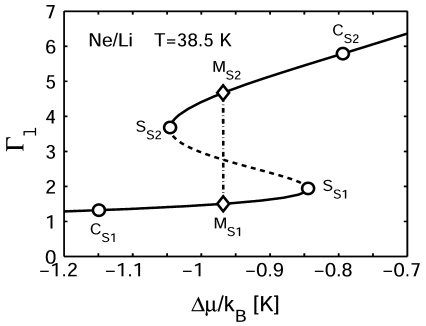

Figure 1. Adsorption isotherm showing results for symmetric solutions for a slit of Li filled with Ne at $T = 38.5$ K. Solid curves were obtained with both the CE and GCE schemes, while the dashed line is obtained in the CE scheme only. Labels S_{S1} and S_{S2} show the location of spinodal points, while C_{S1} and C_{S2} are two generic stable states in the thin and thick film regimes, respectively. M_{S1} and M_{S2} stand for the coexisting thin and thick films determined from the equal-areas Maxwell construction indicated by the dash-dotted line.

obtained with both the GCE and CE calculations. Notice that the GCE scheme only provides solutions with positive slope $d\mu/dn$ guaranteeing convexity of F_{DF}. This property is also exhibited by variational microscopic calculations performed in the framework of the paired-phonon analysis in conjunction with the hyper-netted chain expansion.[45−48] Between the spinodal points S_{S1} and S_{S2} (characterized by $d\Delta\mu/d\Gamma_l = d\mu/dn = 0$), there is a regime marked by a dashed curve where F_{DF} is not convex exhibiting $d\mu/dn < 0$. These data were obtained from CE calculations.

The fact that at each step of the CE scheme $\rho(z)$ is normalized to the required number of particles means that within this statistics one needs a smaller number of iterations than in the GCE case to get convergence. Therefore, the CE scheme is widely used in the literature to study adsorption. A theoretical justification for the broad use of CE was provided by White et al.[49] These authors have shown that for stable or metastable solutions the results of the GCE and CE statistics may differ only if one considers situations of extreme confinement with a small number of particles.

The CE scheme provides $\Delta\mu(T)$ for all values of n. When in this frame the data exhibit S-shaped van der Waals isotherms,[50−54] the two coexisting stable states (thin and thick films) located at n_{thin} and n_{thick} (i.e., at $\Gamma_{l,thin}$ and $\Gamma_{l,thick}$, respectively) satisfying

$$\mu(n_{thin}) = \mu(n_{thick}) = \mu_{eq}(\Omega_{eq}/A) \tag{3.1}$$

are determined by applying the Maxwell rule of equal areas as in refs 25, 50, and 52

$$\int_{n_{thin}}^{n_{thick}} [\mu(T) - \mu_0(T)]\, dn = \Delta\mu_{pw}(T)[n_{thick} - n_{thin}] \tag{3.2}$$

This Maxwell construction is depicted in Figure 1, where the points M_{S1} and M_{S2} stand for symmetric states which films formed at both walls coincide, respectively, with the thin and thick structures got at coexistence for adsorption on a single wall.

In the case of substrates with intermediate strength, for $n \leq n_{thin}$, the system grows continuously and, for $n \geq n_{thick}$ (i.e., for $\Gamma_l \geq \Gamma_{l,thick}$), the film's growth does not present any further jump in coverage.

In the case of the GCE scheme, due to the lack of data in the non-convex region, it is impossible to apply the equal area Maxwell rule given by eq 3.2. Hence, some alternative method should be utilized to get the coexisting states. In the following lines, we shall outline an adequate procedure based on thermodynamics.

For a surface system at fixed T, thermodynamic relations yield for the chemical potential[27,47,48]

$$\mu = \left(\frac{\partial F}{\partial N}\right)_{T,A} = f + n\frac{\partial f}{\partial n} = f - \frac{1}{n}\frac{\partial f}{\partial n^{-1}} \tag{3.3}$$

and for the surface energy per unit area σ_A

$$\sigma_A = \left(\frac{\partial F}{\partial A}\right)_{T,N} = \frac{\partial f}{\partial n^{-1}} = -n^2\frac{\partial f}{\partial n} = n(f - \mu)$$
$$= \frac{F - \mu N}{A} = \frac{\Omega}{A} = \omega \tag{3.4}$$

The equilibrium condition for a single-component fluid at T is that μ be uniform throughout the system. Two phases can coexist at a given T if and only if both phases have the same μ and ω as required by eq 3.1. From a set $[n, \mu, f]$ obtained in the convex regime of F, i.e., along the sectors C_{S1}−S_{S1} and S_{S2}−C_{S2} of the curves traced in Figure 1, one can evaluate the corresponding ω. In turn, these data can be used to perform the "so-called" tangent Maxwell construction.[50,51] This method is based upon drawing tangent lines y to the curves of f vs n^{-1} for both sectors C_{S1}−S_{S1} and S_{S2}−C_{S2}. Since according to eq 3.4 the tangent $(\partial f/\partial n^{-1})$ is equal to ω, at coexistence it must hold

$$\omega_{eq} = \left(\frac{\partial f}{\partial n^{-1}}\right)_{n_{thin}} = \left(\frac{\partial f}{\partial n^{-1}}\right)_{n_{thick}} \tag{3.5}$$

Starting from the slope of the straight line y which matches coexisting points of f at $1/n_{thin}$ and $1/n_{thick}$, one may arrive at

$$y = f(n_{thin}) + \left(\frac{\partial f}{\partial n^{-1}}\right)_{n_{thin}} (n^{-1} - n_{thin}^{-1})$$
$$= f(n_{thick}) + \left(\frac{\partial f}{\partial n^{-1}}\right)_{n_{thick}} (n^{-1} - n_{thick}^{-1}) \tag{3.6}$$

dx.doi.org/10.1021/jp4000895 | J. Phys. Chem. B 2013, 117, 6256−6268

Since two coexisting layers must exhibit the same μ and ω, then tangent lines for both layers coincide. Hence, by using eqs 3.3 and 3.4, one gets

$$y = \mu(n_{thin}) + \omega(n_{thin})n^{-1} = \mu(n_{thick}) + \omega(n_{thick})n^{-1} = \mu_{eq} + \omega_{eq}n^{-1} \quad (3.7)$$

From this matching condition, one can determine μ_{eq}, ω_{eq}, and densities n_{thin} and n_{thick}. However, the outlined tangent Maxwell construction is not the most used procedure for determining a phase transition.

An alternative way consists of using the known μ and ω as a function of n for plotting ω vs $\Delta\mu$ for both phases and determining μ_{eq} and ω_{eq} at coexistence from the crossing. See, for instance, the crossing diagrams displayed in Figure 3 of ref 47, Figures 2–4 of ref 55, and the zigzag construction drawn in Figure 2 of ref 56. Our data with positive $d\mu/dn$ (obtained in both CE and GCE schemes) are plotted in Figure 2, where the

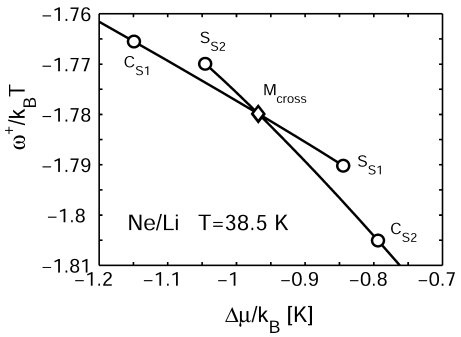

Figure 2. Grand potential per unit area as a function of the chemical potential for a slit of Li filled with Ne at T = 38.5 K. The data correspond to solid lines in Figure 1. Here we define $\omega^+ = \omega\tilde{\sigma}_{ff}^2$. The curve containing the points C_{S1} and S_{S1} represents thin films, while that with S_{S2} and C_{S2} stands for thick films. The crossing point labeled by M_{cross} indicates coexisting films.

point labeled by M_{cross} indicates $\Delta\mu_{pw}(T)$ [$=\mu_{eq} - \mu_0(T)$] and ω_{eq} at coexistence. At this crossing point, there is a characteristic knee of a first-order transition. Of course, the values of $\Delta\mu_{pw}(T)$ obtained in Figures 1 and 2 coincide. Moreover, the points M_{S1} and M_{S2} merge into M_{cross}. The states along the C_{S1}–M_{cross}–C_{S2} line are stable, while those lying in the sectors M_{cross}–S_{S1} and S_{S2}–M_{cross} are metastable. According to Hansen and McDonald, this kind of metastable states could be reached experimentally if sufficient care is taken to prevent formation of the thermodynamically stable phase (see Chapter 5.6 in ref 39) and in such a way hysteresis cycles may be obtained. More details about measurements of states located along S-shaped isotherms can be found in refs 53 and 54.

The numerical consistence between results obtained from the procedure displayed in Figure 2 and the "pure" tangent-based Maxwell construction was checked. The difference between the evaluated f_{DF} and the straight line y of eq 3.7 is plotted in Figure 3 as a function of $1/n^*$. This difference becomes zero at $1/n^*_{thin}$ and $1/n^*_{thick}$ as required by eq 3.6.

III.2. Prewetting lines and wetting temperatures from symmetric solutions. In the present work, we determine wetting properties from the analysis of energetics of the symmetric solutions. In order to perform this kind of analysis, the width of slits should be sufficiently large to guarantee that at a given T the density ρ_B of vapor formed in the central region

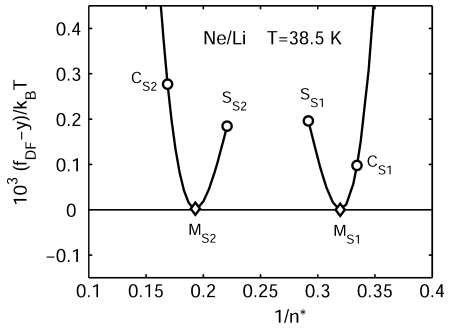

Figure 3. The difference between the evaluated f_{DF} and the straight line y given by eq 3.7 as a function of $1/n^*$ for a slit of Li filled with Ne at T = 38.5 K. This difference becomes zero at coexisting inverse coverages $1/n^*_{thin}$ and $1/n^*_{thick}$. The meaning of the set of labeled points is the same as in Figure 1.

be equal to the asymptotic density obtained in the adsorption on a single wall. The considered widths L^* = 40 for Ne/Li and Ne/Na and L^* = 60 for Ne/Rb satisfy this condition. The main results are displayed in Figure 4; these data were calculated in both the CE and GCE schemes.

Figure 4a shows adsorption isotherms for Ne/Li evaluated at several temperatures above T_w. Vertical lines indicate $\Delta\mu_{pw}(T)$ determined from Maxwell constructions described above. One may observe the evolution of the PW phenomenon characterized by the jump in coverage $\Delta\Gamma_l = \Gamma_{l,thick} - \Gamma_{l,thin}$ at $\Delta\mu_{pw}(T)$. The largest jump occurs close to T_w, then it shrinks for increasing T, and it eventually disappears at T_{cpw} where the thin and thick films merge. Thus, $\Delta\Gamma_l$ serves as an order parameter which vanishes at the critical prewetting point obeying a power law[52]

$$\Delta\Gamma_l(T) = b_{pw}(T_{cpw} - T)^{1/2} \quad (3.8)$$

the critical exponent 1/2 corresponds to the MFA adopted in the present work for the atractive f–f interaction and b_{pw} is a model parameter. Figure 4b shows $\Delta\mu_{pw}$ as a function of temperature. This simple PW line corresponds to the case depicted in panel b of Figure 1 in ref 5, and it has been measured in several systems.[57] The relative chemical potential $\Delta\mu_{pw}$ approaches tangentially zero at T_w; thermodynamic arguments[5] lead to the form

$$\Delta\mu_{pw}(T) = \mu_{pw}(T) - \mu_0(T) = a_{pw}(T - T_w)^{3/2} \quad (3.9)$$

with a_{pw} being a model parameter. In practice, this expression is used to fit data of $\Delta\mu_{pw}(T)$ for determining T_w. A fit of data displayed for Ne/Li in Figure 4b yielded T_w = 35.9 K and $a_{pw}/k_B = -0.22$ K$^{-1/2}$. In addition, from eq 3.8, we got T_{cpw} = 38.8 K and b_{pw} = 5.9 K$^{-1/2}$.

Adsorption isotherms for the Ne/Na system are displayed in Figure 4c, and $\Delta\mu_{pw}$ vs T is plotted in Figure 4b. Fitting the latter data to eq 3.9, one gets a PW line with parameters T_w = 39.6 K and $a_{pw}/k_B = -0.23$ K$^{-1/2}$. The use of eq 3.8 yielded the CPW point at T_{cpw} = 41.2 K with b_{pw} = 9.5 K$^{-1/2}$.

Adsorption isotherms calculated for Ne/Rb are shown in Figure 4d, and the corresponding $\Delta\mu_{pw}$ vs T is included in Figure 4b. In the case of this system, we obtained T_w = 42.25 K and $a_{pw}/k_B = -0.24$ K$^{-1/2}$ for the PW line and T_{cpw} = 43.02 K with b_{pw} = 13.9 K$^{-1/2}$ for the CPW point.

The PW lines displayed in Figure 4b are in good agreement with those previously obtained from the analysis of adsorption

dx.doi.org/10.1021/jp4000895 | J. Phys. Chem. B 2013, 117, 6256–6268

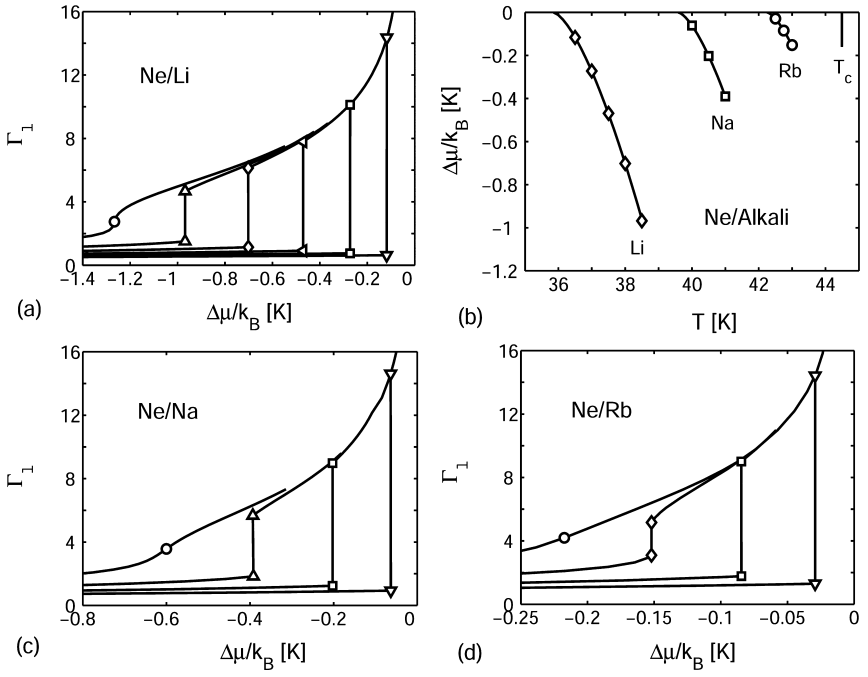

Figure 4. (a) Adsorption isotherms for a slit of Li filled with Ne as a function of coverage Γ_l at temperatures from 36.5 K (down triangles) to 39 K (circle) in steps of 0.5 K. (b) PW lines for the Ne/Li (diamonds), Ne/Na (squares), and Ne/Rb (circles) systems. (c) Same as part a but for Ne/Na at T from 40 K (down triangles) to 41.5 K (circle) in steps of 0.5 K. (d) Same as part a but for Ne/Rb at T from 42.5 K (down triangles) to 43.25 K (circle) in steps of 0.25 K.

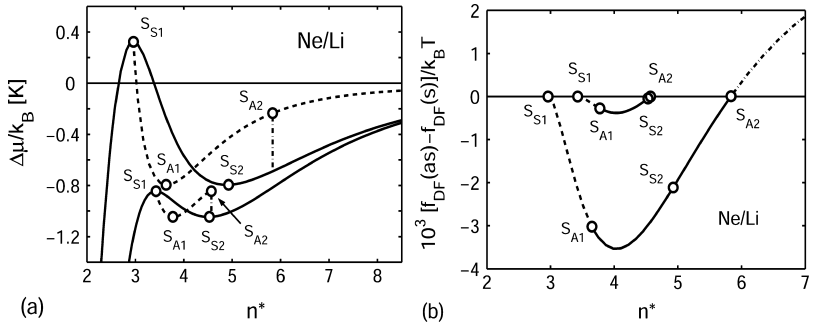

Figure 5. (a) Reduced chemical potential for symmetric (solid curves) and asymmetric (dashed curves) solutions at two temperatures, starting from the top T = 37.5 and 38.5 K, as a function of the dimensionless number of particles per area. For the meaning of labels S_{S1}, S_{S2}, and S_{A1}, see the text. Vertical dash-dotted lines indicate the largest n^* at which SSB occurs. (b) Difference between free energies per particle of asymmetric and symmetric solutions obtained in the CE frame at T = 37.5 K (lower curve) and 38.5 K (upper curve) as a function of n^*. In the regime delimited by S_{S1} and S_{A1}, the chemical potential of asymmetric solutions exhibits a negative slope, and above $n^*(S_{A1})$, the slope becomes positive; the latter results are also obtained in the GCE scheme.

on a single wall (cf. Figure 5 of ref 30). The values of T_w given above are in concordance with that quoted in Table 1 of ref 30. These facts confirm that the width of adopted slits is sufficiently large for studying wetting properties. The conclusions obtained from comparisons of present results with those of previous DF calculations of Ancilotto and Toigo[22] and GCMC simulations of Curtarolo et al.[58] remain the same as that already reported in ref 30. Therefore, here we shall restrict ourselves to stress that our calculations predict wetting of Rb by Ne with a T_w close to T_c in agreement with the experimental result of Hess, Sabatini, and Chan.[59]

III.3. Asymmetric Solutions. Symmetry breaking solutions are obtained for both closed and open slits, which are treated by applying CE and GCE statistics, respectively. Above T_w, asymmetric solutions occur along PW lines.

III.3.1. Closed Slits - Canonical Ensemble. Let us now focus on the analysis of asymmetric solutions obtained for the filling of closed slits studied by applying the CE statistics keeping fixed the set [n, T, V], as described in section II.2.2. In a first step, we shall examine in some detail two adsorption isotherms obtained for a slit of Li at T = 37.5 and 38.5 K. These data are displayed in Figure 5a. Symmetric solutions are indicated by solid curves running over the points S_{S1} and S_{S2}, while asymmetric ones are represented by dashed curves starting at points S_{S1} and running over spinodal points of asymmetric solutions S_{A1}. Thus, asymmetric solutions just begin at the maximum of $\Delta\mu_{sym}$, i.e., asymmetry appears in the region where the slope $d\Delta\mu_{sym}/dn$ becomes negative, while the slope of μ_{asym} is positive over a large portion of that region satisfying the stability condition there. The regime with positive slope $d\Delta\mu_{asym}/dn$ begins at S_{A1}, where the free energy F_{DF}(asym)

dx.doi.org/10.1021/jp4000895 | J. Phys. Chem. B 2013, 117, 6256−6268

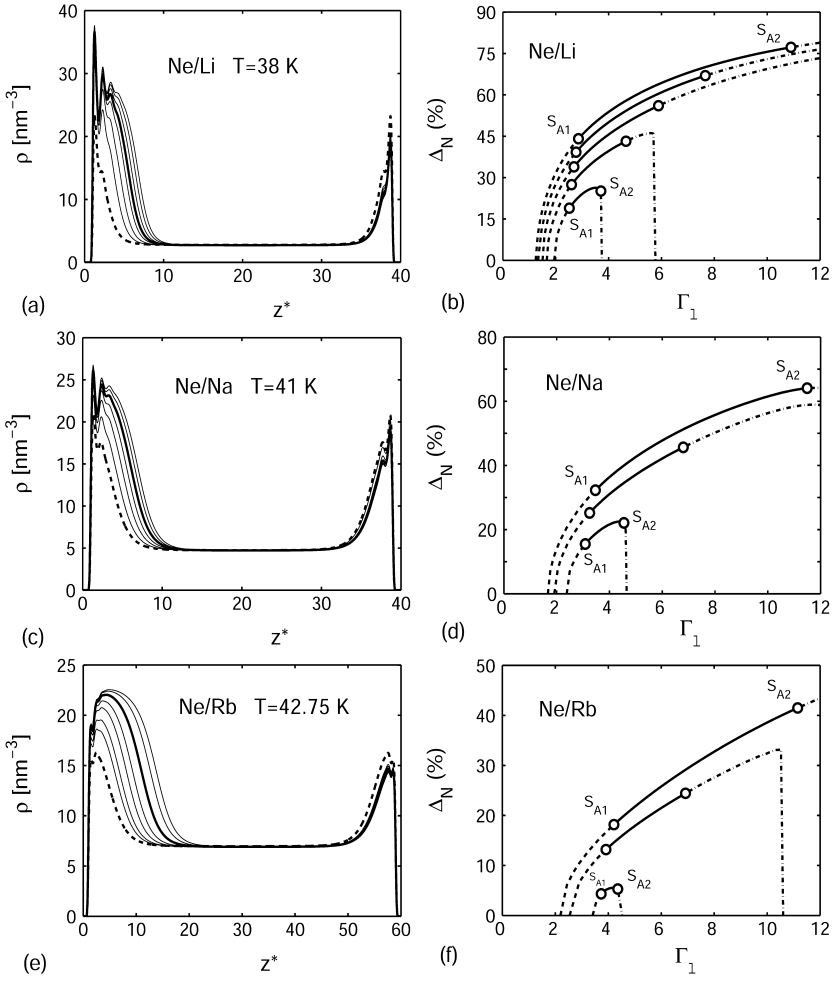

Figure 6. (a) Asymmetric density profiles of Ne in a closed slit of Li at T = 38 K for several coverages Γ_l. The fat curve is the asymmetric profile which coexists with symmetric ones (see text). The dashed curve is the largest metastable thin symmetric profile. (b) Asymmetry parameter for Ne/Li as a function of coverage at temperatures from 36.5 K (highest curve) to 38.5 K (lowest curve) in steps of 0.5 K. The meaning of points S_{A1} and S_{A2} is that of Figure 5. (c) Same as part a but for Ne/Na at T = 41 K. (d) Same as part b but for Ne/Na at T from 40 K (highest curve) to 41 K (lowest curve) in steps of 0.5 K. (e) Same as part a but for Ne/Rb at T = 42.75 K. (f) Same as part b but for Ne/Rb at T from 42.5 K (highest curve) to 43 K (lowest curve) in steps of 0.25 K.

becomes a convex function of n. Notice that there is an important qualitative difference between results for asymmetric species at these temperatures. The clue is that at T = 37.5 K the reduced chemical potential at S_{S1} is positive, while at 38.5 K it is negative. This fact causes that at the later temperature the regime of occurrence of asymmetric solutions finishes when $\Delta\mu_{asym}$ reaches the value of $\Delta\mu_{sym}$ obtained at S_{S1}. On the other hand, at T = 37.5 K, $\Delta\mu_{asym}$ of asymmetric states approaches zero from below until eventually the transition to capillary condensation occurs.

The difference between free energies per particle, $f_{DF} = F_{DF}/N$, of asymmetric and symmetric solutions obtained at T = 37.5 and 38.5 K is displayed as a function of n^* in Figure 5b. The asymmetric solutions have lower free energies than the symmetric ones over the entire range S_{S1}–S_{A1}–S_{S2}–S_{A2}. States along the dashed sector of the curve between S_{S1} and S_{A1} exhibit a negative slope $d\Delta\mu_{asym}/dn$, indicating a negative compressibility and sometimes are called internal states.[56]

It is important to mention that between S_{S1} and S_{A1} the symmetry breaking is always obtained spontaneously; i.e., even when the calculations are initialized with symmetric inputs, the iterations lead to asymmetric solutions. Moreover, in order to get symmetric profiles in this regime of n^*, one must impose symmetry at each step of the procedure. This behavior resembles the finding reported in ref 21 where the symmetry breaking was spontaneous within the dynamics and did not have to be seeded. On the other hand, in the regime from S_{S2} to S_{A2}, the asymmetric profiles have to be seeded, whereas between S_{A1} and S_{S2} the pattern is not well-defined.

In order to facilitate a comparison between asymmetric solutions for different absorbers, selected asymmetric profiles are displayed in a compact manner in Figure 6. Thus, panels a, c, and e depict the growth of asymmetric $\rho(z)$ at a fixed T for Li, Na, and Rb, respectively. The degree of asymmetry of the density profiles is measured by the coefficient

$$\Delta_N(\%) = \frac{100}{n_c}\int_0^{L/2} dz([\rho(z) - \rho_B] - [\rho(L - z) - \rho_B]) \quad (3.10)$$

In fact, there are two energetically equivalent asymmetric solutions which satisfy $\rho_{asym2}(z) = \rho_{asym1}(L - z)$, yielding $\Delta_N[\rho_{asym2}] = -\Delta_N[\rho_{asym1}]$. Calculated asymmetry coefficients

dx.doi.org/10.1021/jp4000895 | J. Phys. Chem. B 2013, 117, 6256–6268

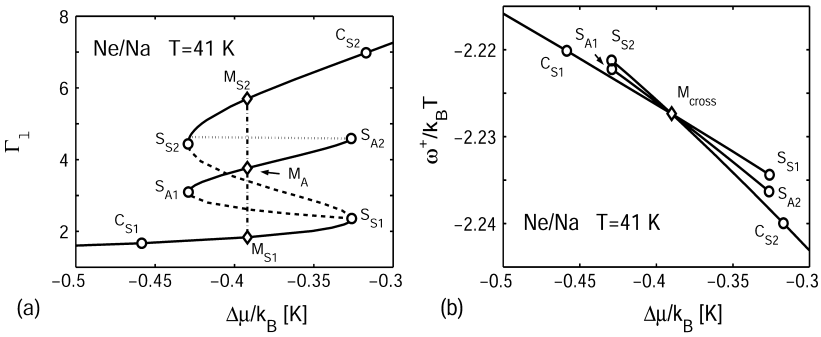

Figure 7. (a) Adsorption isotherm for symmetric and asymmetric solutions plotted as coverage Γ_l versus reduced chemical potential. The symmetric solutions go through the set of points (C_{S1}, S_{S1}, S_{S2}, C_{S2}), while the asymmetric ones join the points (S_{S1}, S_{A1}, S_{A2}, S_{S2}). The vertical dash-dotted line is the Maxwell construction joining the symmetric stable coexisting states M_{S1} and M_{S2}, while M_A stands for the asymmetric stable coexisting state (see text). (b) Grand free energy per unit one wall area as a function of reduced chemical potential for symmetric and asymmetric solutions. The meaning of the points (C_{S1}, S_{S1}, S_{A1}, S_{A2}, S_{S2}, C_{S2}) is the same as in panel a. The symmetric solutions lay on the curves C_{S1}–S_{S1} and S_{S2}–C_{S2}, while the asymmetric solution determines the line S_{A1}–S_{A2}. The point M_{cross} indicates the location of the crossing of the three lines determining the coexistence of symmetric and asymmetric solutions labeled, respectively, by M_{S1}, M_{S2}, and M_A in panel a.

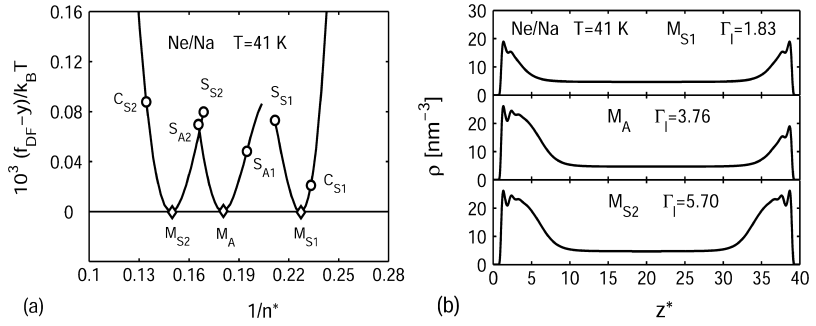

Figure 8. (a) The difference between the evaluated f_{DF} and the straight line y given by eq 3.7 as a function of $1/n^*$ for a slit of Na filled with Ne at T = 41 K. The meaning of the marked points is the same as that in Figure 7. This difference becomes zero at inverse coverages of coexisting symmetric and asymmetric states. (b) Density profiles of Ne confined in a slit of Na as a function of z^*. These data correspond to coexisting systems at T = 41 K. Both the CE and GCE statistics provide these results. The labels M_{S1} and M_{S2} indicate symmetric solutions, while M_A indicates the asymmetric one.

Δ_N for $T \geq T_w$ are shown in panels b, d, and f of Figure 6 as a function of coverage.

Figure 6a shows the asymmetric filling of a slit of Li at T = 38 K between the states S_{S1} and S_{A2} defined before. Looking at the growth of the thick film for increasing Γ_l, one may observe that it reaches the saturation liquid density. The asymmetry coefficients for the examined temperatures above T_w are plotted in Figure 6b. Three regimes are individualized for every one of the displayed curves. From its beginning up to S_{A2}, as mentioned previously, the asymmetric solutions satisfy $f_{DF}(\text{asym}) - f_{DF}(\text{sym}) < 0$; above $\Gamma_l(S_{A2})$, the sign of this difference is reversed. Below $\Gamma_l(S_{A1})$, the slope $d\Delta\mu_{asym}/dn$ is negative, while between S_{A1} and S_{A2} this slope becomes positive. On the other hand, a view at Figure 6b indicates the following for increasing T: (i) the asymmetric $\rho(z)$ appears at larger coverages, and (ii) the coverage's range where $f_{DF}(\text{asym}) - f_{DF}(\text{sym}) < 0$ diminishes. Furthermore, these structures can be related to the corresponding PW line in the displayed in Figure 4b. The SSB effect is present along the PW line until it eventually disappears at a critical temperature T_{ssb} which coincides with T_{cpw}.

In the case of Ne/Na, asymmetric profiles obtained at T = 41 K are plotted in Figure 6c and asymmetry coefficients are displayed in Figure 6d. Finally, asymmetric profiles calculated for Ne/Rb at T = 42.75 K are shown in Figure 6e, while asymmetry coefficients for this system are given in Figure 6f. The overall characteristics of results for the systems Ne/Na and Ne/Rb are similar to that found for Ne/Li. The main difference is that for Rb, which is the weakest studied substrate, the profiles do not show typical peaks denoting layering close to the walls.

In summary, we can state that a comparison of all the asymmetry coefficients displayed in Figure 6 to the first-order transition lines depicted in a (T, $\Delta\mu$) plane in Figure 4b indicates that for all substrates the SSB effect extends along PW lines terminating at a critical T_{ssb} in concordance with T_{cpw}.

III.3.2. Open Slits - Grand Canonical Ensemble. Open slits are also in thermodynamic equilibrium with an environment at fixed T, but in this case, the confined system is exposed to an unrestricted fluid exchange with the reservoir at fixed μ. Under such circumstances, the adsorption occurs at a constant set [μ, V, T]. As mentioned before, this kind of system is studied by applying GCE.

Let us now comment in detail on the results obtained for Ne/Na at T = 41 K. This value is the highest temperature exhibiting a first-order transition. The corresponding adsorption isotherm calculated with both the CE and GCE schemes is displayed in Figure 7a, where the equal-areas Maxwell construction performed with symmetric CE solutions is also shown. All the states marked with solid lines were obtained from both CE and GCE schemes. Hence, GCE **does** provide

dx.doi.org/10.1021/jp4000895 | J. Phys. Chem. B 2013, 117, 6256–6268

both symmetric and asymmetric solutions in the regimes where the corresponding Helmholtz free energy, F_{DF}, is convex, yielding positive $d\Delta\mu/dn$. The lack of GCE data in the nonconvex region makes it necessary to apply the tangent Maxwell construction for seeking out the coexisting states. Figure 7b shows ω as a function of $\Delta\mu$ for both symmetric and asymmetric solutions with positive $d\Delta\mu/dn$ displayed in Figure 7a. The crossing of the lines labeled by $C_{S1}-S_{S1}$ and $S_{S2}-C_{S2}$ in Figure 7b occurs at M_{cross} and determines the coexisting symmetric solutions M_{S1} and M_{S2} already identified in Figure 7a. Furthermore, the line $S_{A1}-S_{A2}$ corresponding to asymmetric solutions crosses the symmetric ones also just at M_{cross}; i.e., this point is indeed determined by the intersection of three lines in Figure 7b. Hence, the state M_A quoted in Figure 7a has the same equilibrium grand free energy per unit area, ω_{eq}, like the coexisting symmetric states M_{S1} and M_{S2}. All three of these phases satisfy the equilibrium condition

$$\Delta\mu_{S1}(T, \omega_{eq}) = \Delta\mu_{S2}(T, \omega_{eq}) = \Delta\mu_{A}(T, \omega_{eq}) = \Delta\mu_{eq}(T, \omega_{eq}) \quad (3.11)$$

where $\Delta\mu_{eq}(T, \omega_{eq}) = -0.3899$ K with $\omega_{eq}/k_BT = -32.90$ nm^{-2}. The density profile of the state M_A is marked with a fat line in Figure 6c.

It is worth mentioning what happens when in the unstable region from S_{S1} to S_{A1} if one carries out a GCE calculation taking the CE asymmetric solution as a starting point. In the GCE scheme, μ is kept fixed; hence, the solution will move changing Γ_l along a vertical line in Figure 7a until either the $C_{S1}-S_{S1}$ curve or the $S_{A1}-S_{A2}$ one can be reached. The result will depend on the landscape of the free energy.

For the sake of completeness, we also produced a drawing similar to Figure 3 but including all three coexisting states. Thus, Figure 8a shows differences between the Helmholtz free energy per particle for the sectors displayed in Figure 7b and the straight line given by eq 3.7, i.e., $y = \mu_{eq} + \omega_{eq}n^{-1}$, evaluated with $\mu_{eq}/k_BT = -6.972$ [$\mu_0/k_BT(T = 41$ K$) = -6.963$] and $\omega^+_{eq}/k_BT = -2.227$. One may realize that the three "parabolas" come into contact with the horizontal zero line just at the coexisting points M_{S1}, M_A, and M_{S2}. Hence, there is complete agreement among the results extracted from data of Figures 7a, 7b, and 8a.

The density profiles of the states M_{S1}, M_A, and M_{S2} are compared in Figure 8b. In the case of M_A, the spectrum exhibits at the right wall the coexisting thick wetting film and at the other wall the coexisting thin one. However, it should be stressed that the asymmetric solution is twofold; there is another asymmetric profile which presents a thin film at the right wall and a thick film at the left one and has the same energetics like the plotted one.

It is important to notice that the data plotted in Figure 7b indicate that, away from M_{cross} for each value of $\Delta\mu$, the asymmetric metastable states always have a lower grand potential energy, ω, than the symmetric metastable ones. On the other hand, it is well-known that above T_w for a given μ the states with lowest grand potential lie on the line determined by $C_{S1}-M_{cross}-C_{S2}$ and wetting implies that the structures of the states are uniform films over the (x, y) plane. Therefore, no structure breaking symmetry on the (x, y) plane would have lower ω at μ_{eq} than the coexisting symmetric and asymmetric states obtained at M_{cross}. For temperatures in the range $T_w < T < 41$ K, the Ne/Na system also exhibits M_{cross} points denoting coexisting symmetric and asymmetric states. The features exhibited by the isotherms for Ne/Na were also found in the cases of the Ne/Li and Ne/Rb systems. Asymmetric coexisting profiles for Ne/Li at $T = 38$ K and for Ne/Rb at $T = 42.75$ K are also marked with fat curves in parts a and e of Figure 6, respectively.

Figure 9 shows the phase diagram for coexisting states at temperatures $T > T_w$ for all the analyzed substrates. These data

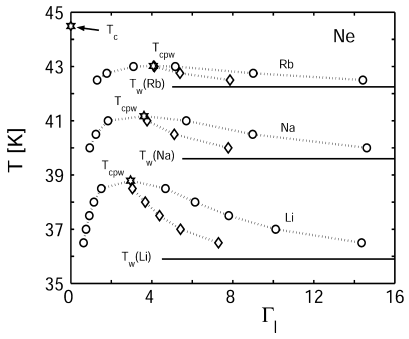

Figure 9. Phase diagram of coexisting states of Ne confined in slits of Li, Na, and Rb at temperatures between T_w and T_{cpw} (all of these temperatures are lower than T_c). These data were obtained with both the CE and GCE statistics. Circles are symmetric states, while diamonds are asymmetric ones. The dotted lines are plotted to guide the eye; these lines merge at the corresponding $T_{ssb} \simeq T_{cpw}$ indicated by stars.

were obtained by applying both the CE and GCE schemes. One may realize that the coverage Γ_l corresponding to the symmetric thick films as well as to the asymmetric ones goes to infinity when the temperature approaches T_w. On the other hand, both symmetric and asymmetric species merge at $T_{ssb} \simeq T_{cpw}$. Above this critical temperature, only one sort of symmetric state is obtained.

Finally, Figure 10 shows the evolution of the coexisting asymmetric profiles as a function of temperature in the range $T_w < T < T_{ssb}$. For decreasing temperatures, one may observe how the thick part of the profile grows, while simultaneously the thin part becomes smaller. It is expected that for $T \to T_w$ the width of asymmetric films will diverge, leading to $\Gamma_l \to \infty$.

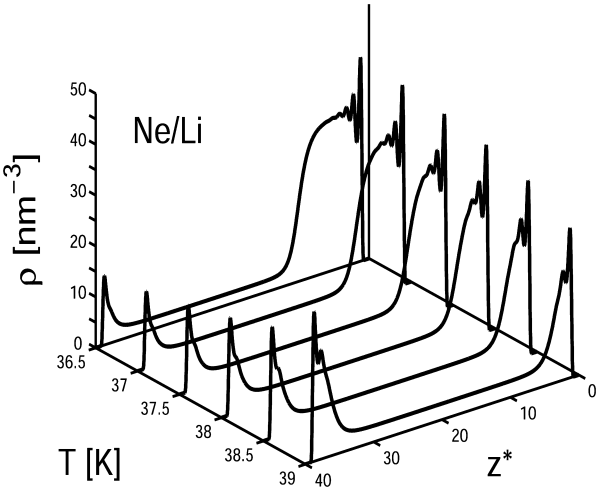

Figure 10. Asymmetric density profiles of Ne confined in a slit of Li as a function of z^* for several values of T. These data correspond to coexisting systems obtained from calculations performed in both the CE and GCE statistics.

dx.doi.org/10.1021/jp4000895 | J. Phys. Chem. B 2013, 117, 6256−6268

All the main features reported in this work remain unchanged when the width of the slit is enlarged.

III.3.3. Discussion of the SSB Effect. In general, the stability of an equilibrium state of confined systems depends on the constraints to which they are subjected. Thus, systems limited to constant overall composition (closed systems) may differ in their stability from those in which particles can unrestrictedly enter or leave the system (open systems). Hence, states which could be stabilized in the closed system (CE) are not necessarily stable in the open system (GCE).

In this paper, we are dealing with a physical phenomenon occurring for a thin to thick film wetting transition. If at a constant temperature in the range $T_w \leq T \leq T_{cpw}$ one increases $n = N/A$ starting from a small value, then a stable thin film will be formed on each wall (symmetric density profile) until the thin−thick film coexistence condition of eq 3.1 can be reached. At this point, by adding more particles, the thin films would enter in a metastable regime competing with the formation of drops at the walls until the spinodal point S_{S1} of Figure 5a is reached. Beyond this point, the symmetric films become unstable, by increasing n in the CE scheme, a thin film at one wall (the right wall in panels a, c, and d of Figure 6) does not grow, remaining at its stable coexisting size, while at the other wall the thicker film grows but with a negative slope $d\Delta\mu_{asym}/dn$; therefore, at the latter wall, the growth of droplets would be preferable. Since by assuming $\rho(\mathbf{r}) = \rho(z)$ the system is forced to be homogeneous along the walls, we only obtain translational invariant layers of liquid even when the system would prefer to phase separate (that is, to form a drop on a wall). As it happens, having one of these unphysical layers on one wall is energetically more favorable than having one at each wall (see Figure 5b). Hence, one would say that such a structure is energetically more favorable than having droplets on both walls. More particles would make these droplets grow until there are enough particles to form the stable thick layer; this could be preceded by formation of a metastable thick film after the point S_{A1} of Figure 7a showing SSB. The coexisting thin and thick films form the asymmetric stable profile marked by M_A in that drawing. According to our CE calculations, further increasing n just makes the thick layer grow as a metastable film exhibiting SSB until a jump to the symmetric profile at S_{A2}. However, such an evolution would compete unfavorably against a structure where the thick wetting layer remains unchanged, while on the other wall droplets grow until a thick wetting film is formed. From that point on, a symmetric profile grows when particles are added. Let us note that Ancilotto et al.[60] showed that, if one approaches the prewetting region from the high coverage regime reducing it gradually, a thick film on one wall can break into low density patches (bubbles) surrounded by high density region remnants of the original film. It is also worth mentioning that, for instance, Berim and Ruckenstein[19] found for a narrow slit with $L^* = 10$ that states breaking symmetry also along the x and/or y direction may have under certain circumstances lower Helmholtz free energy than asymmetric profiles with $\rho(\mathbf{r}) = \rho(z)$.

In the GCE scheme, where no drops can be formed on the walls (even if allowing $\rho(\mathbf{r})$ to depend on x and/or y), we also find asymmetric solutions. The only stable asymmetric profile exhibiting SSB is that formed with *coexisting wetting films*, i.e., a thin wetting layer on one wall and a thick wetting layer on the other, as shown in the structures displayed in Figure 10. The remaining GCE asymmetric solutions (also found in the CE) are metastable and do not fully minimize the grand free energy of the system, as indicated in Figure 7b. In fact, they correspond to having only one wetting layer (in either of the walls), which of course is a better deal than having none but worse than having a wetting layer at each of the walls. Perhaps, these metastable states could be found in adsorption−desorption hysteresis loops.

IV. SUMMARY

The confinement of Ne between two identical parallel planar walls of alkaline metals was investigated within the frame of a DF theory. The CE and GCE statistics were applied to closed and open systems, respectively. The analysis was focused in the wetting regime at a single wall, and it was assumed that the one-body density is homogeneous over the (x, y) plane of the solid walls; hence, the solutions are restricted to density profiles satisfying $\rho(\mathbf{r}) = \rho(z)$. It was found that under certain conditions the E−L equations, besides the expected symmetric solutions, also yield asymmetric ones which exhibit the SSB effect.

Since the width of the analyzed slits is large enough to minimize finite size effects, symmetric solutions are used to identify first-order phase transitions and determine PW lines. Equilibrium chemical potential μ_{eq}, at which stable thin and thick wetting films coexist, were evaluated by building Maxwell constructions. The results provided by the CE and GCE schemes are equivalent. PW lines are used to determine wetting and critical PW temperatures, T_w and T_{cpw}. The values obtained in the present work are consistent with those determined from a study of the adsorption on single walls reported in a previous paper[30] by the authors.

At temperatures higher than T_w, solutions breaking the left−right symmetry of the adsorption potential exerted by the slit appear along PW lines for certain ranges of Γ_l. The filling of closed slits studied by applying the CE scheme indicates that between spinodal points of symmetric solutions the asymmetric profiles exhibit a lower Helmholtz free energy, F_{DF}, than the symmetric ones for the same number of particles per unit area. However, it is not possible to state that this kind of SSB solution fully minimizes F_{DF} because the imposed invariance along the (x, y) plane parallel to the walls prevents formation of drops at the walls. The latter structure may exhibit the lowest F_{DF} along the van der Waals loop according to the physical interpretation of the phenomenon described in section III.3.3. Nevertheless, there exists a range of Γ_l where the asymmetric DF−CE solutions are metastable, as marked in Figures 5 and 6.

Open slits were studied within the GCE frame. All the asymmetric states with positive slope of the chemical potential, i.e., $d\mu/dn > 0$, provided by the CE scheme were also obtained when the GCE was applied. Hence, the asymmetric solutions obtained within the DF−GCE frame are at least metastable and it would be of interest to search whether they could be found in adsorption−desorption hysteresis loops. Maxwell constructions yield three coexisting stable states with the same chemical potential μ and grand free energy potential ω. Two of these states are symmetric, and one is asymmetric but 2-fold degenerate. Symmetric solutions exhibit at both walls either the thin or the thick wetting films obtained at coexistence in the adsorption on a single wall. On the other hand, the asymmetric state shows at one wall the coexisting thick wetting film and at the other wall the corresponding thin one; let us denote this structure the *coexisting asymmetric wetting profile*. These results

dx.doi.org/10.1021/jp4000895 | J. Phys. Chem. B 2013, 117, 6256−6268

indicate that given a sort of *coexisting wetting film* at one wall it is no matter whether at the other wall there is a *thin* or a *thick coexisting wetting film*. This behavior was qualified as conceivable by Merkel and Löwen.[9] It can be explained by the fact that these *thin* and *thick* species are located far away from each other and, therefore, each film acts like in the adsorption on a single wall. Furthermore, it was found that for temperatures in the range $T_w \leq T < T_{cpw}$ there is a one-to-one correspondence between a first-order phase transition line and the occurrence of *coexisting asymmetric wetting profiles*. The concordance between the CPW points where the PW lines terminate and the critical temperatures T_{ssb} at which asymmetric solutions disappear is shown in Figure 9, while the evolution of the *coexisting asymmetric wetting profiles* as a function of temperature for the system Ne/Li is depicted in Figure 10.

In conclusion, the goals of the present work are the following: (i) a detailed description of asymmetric solutions in the convex regimes of F_{DF}, which are mainly metastable; (ii) its relation to PW lines; and (iii) the identification of stable *coexisting asymmetric wetting profiles*. All these results were obtained from DF−CE and DF−GCE calculations carried out with realistic potentials.

AUTHOR INFORMATION

Corresponding Author

*E-mail: szybisz@tandar.cnea.gov.ar.

Notes

The authors declare no competing financial interest.

ACKNOWLEDGMENTS

This work has been supported in part by Grant No. PIP-0546/09 from CONICET and Grants Nos. 01/X099 and 01/K156 from Universidad de Buenos Aires, Argentina.

REFERENCES

(1) de Gennes, P. G. Wetting: Statics and Dynamics. *Rev. Mod. Phys.* **1985**, *57*, 827−863.
(2) Bonn, D.; Eggers, J.; Indekeu, J.; Meunier, J.; Rolley, E. Wetting and Spreading. *Rev. Mod. Phys.* **2009**, *81*, 739−805.
(3) Squires, T. M.; Quake, S. R. Microfluidics: Fluid Physics at the Nanoliter Scale. *Rev. Mod. Phys.* **2005**, *77*, 977−1026.
(4) Pandit, R.; Schick, M.; Wortis, M. Systematics of Multilayer Adsorption Phenomena on Atttractive Substrates. *Phys. Rev. B* **1982**, *26*, 5112−5140.
(5) Pandit, R.; Fisher, M. E. Wetting Transitions near Bulk Triple Points. *Phys. Rev. Lett.* **1983**, *51*, 1772−1775.
(6) Sikkenk, J. H.; Indekeu, J. O.; van Leeuwen, J. M. J.; Vossnack, E. O. Molecular-Dynamics Simulation of Wetting and Drying at Solid-Fluid Interfaces. *Phys. Rev. Lett.* **1987**, *59*, 98−101.
(7) Sikkenk, J. H.; Indekeu, J. O.; van Leeuwen, J. M. J.; Vossnack, E. O.; Bakker, A. F. Simulation of Wetting and Drying at Solid-Fluid Interfaces on the Delft Molecular Dynamics Processor. *J. Stat. Phys.* **1988**, *52*, 23−44.
(8) Tang, J. Z.; Harris, J. G. Fluid Wetting on Molecularly Rough Surfaces. *J. Chem. Phys.* **1995**, *103*, 8201−8208.
(9) Merkel, M.; Löwen, H. Symmetry-Breaking Density Profiles in Confined Liquids. *Phys. Rev. E* **1996**, *54*, 6623−6632.
(10) Berim, G. O.; Ruckenstein, E. Fluid Density Profile and Symmetry Breaking in a Closed Nanoslit. *J. Phys. Chem. B* **2007**, *111*, 2514−2522.
(11) (a) Tarazona, P. Free-Energy Density Functional for Hard Spheres. *Phys. Rev. A* **1985**, *31*, 2672−2679;(b) *32*, 3148 (erratum).
(12) Berim, G. O.; Ruckenstein, E. Symmetry Breaking of the Fluid Density Profiles in Closed Nanoslits. *J. Chem. Phys.* **2007**, *126*, 124503-1−124503-9.
(13) Szybisz, L.; Sartarelli, S. A. Density Profiles of Ar Adsorbed in Slits of CO_2: Spontaneous Symmetry Breaking Revisited. *J. Chem. Phys.* **2008**, *128*, 124702-1−124702-8.
(14) Sartarelli, S. A.; Szybisz, L. Correlation between Asymmetric Profiles in Slits and Standard Prewetting Lines. *Pap. Phys.* **2008**, *1*, 010001-1−010001-9 (also at http://arxiv.org/abs/0909.2244).
(15) Sartarelli, S. A.; Szybisz, L.; Urrutia, I. Spontaneous Symmetry Breaking and First-Order Phase Transitions of Adsorbed Fluids. *Int. J. Bifurcation Chaos* **2010**, *20*, 287−294.
(16) Sartarelli, S. A.; Szybisz, L. Confinement of Ar between Two Identical Parallel Semi-Infinite Walls. *J. Chem. Phys.* **2010**, *132*, 064701-1−064701-8.
(17) Berim, G. O.; Ruckenstein, E. Symmetry Breaking of the Density Distribution of a Quantum Fluid in a Nanoslit. *J. Chem. Phys.* **2009**, *131*, 184707-1−184707-7.
(18) Mayol, R.; Ancilotto, F.; Barranco, M.; Hernández, E. S.; Pi, M. Novel Aspects of Wedge Filling by Liquid Helium. *J. Low Temp. Phys.* **2007**, *148*, 851−855.
(19) Berim, G. O.; Ruckenstein, E. Two-Dimensional Symmetry Breaking of Fluid Density Distribution in Closed Nanoslits. *J. Chem. Phys.* **2008**, *128*, 024704-1−024704-7.
(20) Rżysko, W.; Patrykiejew, A.; Sokołowski, S. Nucleation of Fluids confined between Parallel Walls: A Lattice Monte Carlo Study. *Phys. Rev. E* **2008**, *77*, 061602-1−061602-6.
(21) Edison, J. R.; Monson, P. A. Modeling Relaxation Processes for Fluids in Porous Materials Using Dynamic Mean Field Theory: An Application to Partial Wetting. *J. Low Temp. Phys.* **2009**, *157*, 395−409.
(22) Ancilotto, F.; Toigo, F. Prewetting Transitions of Ar and Ne on Alkali-Metal Surfaces. *Phys. Rev. B* **1999**, *60*, 9019−9025.
(23) Ancilotto, F.; Curtarolo, S.; Toigo, F.; Cole, M. W. Evidence Concerning Drying Behavior of Ne near a Cs Surface. *Phys. Rev. Lett.* **2001**, *87*, 206103-1−206103-4.
(24) Ravikovitch, P. I.; Vishnyakov, A.; Russo, R.; Neimark, A. V. Unified Approach to Pore Size Characterization of Microporous Carbonaceous Materials from N_2, Ar, and CO_2 Adsorption Isotherms. *Langmuir* **2000**, *16*, 2311−2320.
(25) Ravikovitch, P. I.; Vishnyakov, A.; Neimark, A. V. Density Functional Theories and Molecular Simulations of Adsorption and Phase Transitions in Nanopores. *Phys. Rev. E* **2001**, *64*, 011602-1−011602-20.
(26) Zeng, M.; Tang, Y.; Mi, J.; Zhong, C. Improved Direct Correlation Function for Density Functional Theory Analysis of Pore Size Distributions. *J. Phys. Chem. C* **2009**, *113*, 17428−17436.
(27) Szybisz, L.; Sartarelli, S. A. Full Correspondence between Asymmetric Filling of Slits and First-Order Phase Transition Lines. *AIP Adv.* **2011**, *1*, 042146-1−042146-17.
(28) Rosenfeld, Y. Free-Energy Model for the Inhomogeneous Hard-Sphere Fluid Mixture and Density-Functional Theory of Freezing. *Phys. Rev. Lett.* **1989**, *63*, 980−983.
(29) Kierlik, E.; Rosinberg, M. L. Free-Energy Density Functional for Inhomogeneous Hard-Sphere Fluid: Application to Interfacial Adsorption. *Phys. Rev. A* **1990**, *42*, 3382−3387.
(30) Sartarelli, S. A.; Szybisz, L.; Urrutia, I. Adsorption of Ne on Alkali Surfaces Studied with a Density Functional Theory. *Phys. Rev. E* **2009**, *79*, 011603-1−011603-8.
(31) Sartarelli, S. A.; Szybisz, L. Adsorption of Ar on Planar Surfaces Studied with a Density Functional Theory. *Phys. Rev. E* **2009**, *80*, 052602-1−052602-4.
(32) Evans, R. Density Functionals in the Theory of Nonuniform Fluids. In *Fundamentals of Inhomogeneous Fluids*; Henderson, D., Ed.; Decker: New York, 1992; Chapter 3.
(33) Hohenberg, P.; Kohn, W. Inhomogeneous Electron Gas. *Phys. Rev.* **1964**, *136*, B864−B871.

(34) Roth, R.; Evans, R.; Lang, A.; Kahl, G. Fundamental Measure Theory for Hard-Sphere Mixture Revisited: the White Bear Version. *J. Phys.: Condens. Matter* **2002**, *14*, 12063−12078.
(35) Mansoori, G. A.; Carnahan, N. F.; Starling, K. E.; Leland, T. W., Jr. Equilibrium Thermodynamic Properties of the Mixture of Hard Spheres. *J. Chem. Phys.* **1971**, *54*, 1523−1525.
(36) Weeks, J. D.; Chandler, D.; Andersen, H. C. Role of Repulsive Forces in Determining the Equilibrium Structure of Simple Liquids. *J. Chem. Phys.* **1971**, *54*, 5237−5247.
(37) Lemmon, E. W.; McLinden, M. O.; Friend, D. G. *NIST Chemistry WebBook, NIST Standard Reference Database Number 69*; Linstrom, P. J., Mallard, W. G., Eds.; National Institute of Standards and Technology: Gaithersburg, MD; http://webbook.nist.gov.
(38) Rabinovich, V. A.; Vasserman, A. A.; Nedostup, V. I.; Veksler, L. S. *Thermophysical Properties of Neon, Argon, Krypton, and Xenon*; Hemisphere: Washington, DC, 1988.
(39) Hansen, J.-P.; McDonald, I. R. *Theory of Simple Fluids*; Elsevier: Amsterdam, The Netherlands, 2006; p 304.
(40) Sokołowski, S.; Stecki, J. Second Surface Virial Coefficient for Argon Adsorbed on Graphite. *J. Phys. Chem.* **1981**, *85*, 1741−1746.
(41) Guggenheim, E. A. The Principle of Corresponding States. *J. Chem. Phys.* **1945**, *13*, 253−261.
(42) Chizmeshya, A.; Cole, M. W.; Zaremba, E. Weak Biding Potentials and Wetting Transitions. *J. Low Temp. Phys.* **1998**, *110*, 677−682.
(43) Sinanoğlu, O.; Pitzer, K. S. Interactions between Molecules Adsorbed on a Surface. *J. Chem. Phys.* **1960**, *32*, 1279−1288.
(44) Bruch, L. W.; Cole, M. W.; Zaremba, E. *Physical Adsorption: Forces and Phenomena*; Clarendon Press: Oxford, U.K., 1997; Chapter 2.3.2.2.
(45) Szybisz, L.; Ristig, M. L. New Method of Solving the Optimized Paired-Phonon Analysis Equations and Stability of Thin Films of Liquid ^{4}He at T = 0 K. *Phys. Rev. B* **1989**, *40*, 4391−4404.
(46) Clements, B. E.; Krotscheck, E.; Lauter, H. J. Growth Instability in Helium Films. *Phys. Rev. Lett.* **1993**, *70*, 1287−1290.
(47) Saslow, W. M.; Agnolet, G.; Campbell, C. E.; Clements, B. E.; Krotscheck, E. Theory of First-Order Layering Transitions in Thin Helium Films. *Phys. Rev. B* **1996**, *54*, 6532−6538.
(48) Szybisz, L. Confirmation Using Monte Carlo Ground-State Energies of the Instability of Free Planar Films of Liquid ^{4}He at T = 0 K. *Phys. Rev. B* **1998**, *58*, 109−112.
(49) White, J. A.; González, A.; Román, F. L.; Velasco, S. Density-Functional Theory of Inhomogeneous Fluids in the Canonical Ensemble. *Phys. Rev. Lett.* **2000**, *84*, 1220−1223.
(50) Huang, K. *Statistical Mechanics*; Wiley: New York, 1963; Chapter 2.
(51) Debenedetti, P. G. *Metastable Liquids: Concepts and Principles*; Princeton University Press: Princeton, NJ, 1996; Chapter 2.
(52) Evans, R. Fluids Adsorbed in Narrow Pores: Phase Equilibria and Structure. *J. Phys.: Condens. Matter* **1990**, *2*, 8989−9007.
(53) Amarasekera, G.; Scarlett, M. J.; Mainwaring, D. E. High-Resolution Adsorption Isotherms of Microporous Solids. *J. Phys. Chem.* **1996**, *100*, 7580−7585.
(54) Everett, D. Thermodynamic Stability in Dispersive Systems. *Colloids Surf., A* **1998**, *141*, 279−286.
(55) Nicolaides, D.; Evans, R. Monte Carlo Study of Phase Transitions in a Confined Lattice Gas. *Phys. Rev. B* **1989**, *39*, 9336−9342.
(56) Neimark, A. V.; Ravikovitch, P. I.; Vishnyakov, A. Inside the Hysteresis Loop: Multiplicity of Internal States in Confined Fluids. *Phys. Rev. E* **2002**, *65*, 031505-1−031505-6.
(57) Saam, W. F. Wetting, Capillary and More. *J. Low Temp. Phys.* **2009**, *157*, 77−100.
(58) Curtarolo, S.; Stan, G.; Bojan, M. J.; Cole, M. W.; Steele, W. A. Threshold Criterion for Wetting at the Triple Point. *Phys. Rev. E* **2000**, *61*, 1670−1675.
(59) Hess, G. B.; Sabatini, M. J.; Chan, M. H. W. Nonwetting of Cesium by Neon near Its Critical Point. *Phys. Rev. Lett.* **1997**, *78*, 1739−1742.
(60) Ancilotto, F.; Barranco, M.; Hernández, E. S.; Pi, M. Helium in Nanoconfinement: Interplay between Geometry and Wetting Behavior. *J. Low Temp. Phys.* **2009**, *157*, 174−205.